

Electronic structure of metal hydrides. III. Photoelectron spectroscopy studies of ScH_2 , YH_2 , and LuH_2

J. H. Weaver

Synchrotron Radiation Center, University of Wisconsin-Madison, Stoughton, Wisconsin 53589

D. T. Peterson

Ames Laboratory USDOE and Department of Materials Science and Engineering, Iowa State University, Ames, Iowa 50011

R. L. Benbow

Department of Physics, Northern Illinois University, DeKalb, Illinois 60115

(Received 7 May 1979)

Photoelectron spectroscopy with synchrotron radiation has been used to examine the electronic energy bands of $\text{ScH}_{1.85}$, $\text{YH}_{1.73}$, and $\text{LuH}_{1.77}$ for $15 \leq h\nu \leq 100$ eV. The $h\nu$ -dependent features in the bonding band are discussed in terms of initial-state densities of state and variations in the partial photoionization cross sections. The photoelectron spectroscopy results are combined with those of our earlier optical studies and are used to assess quantitatively the validity of the one-electron band model for d -band metal dihydrides. Good overall agreement is found when compared to the results of recent calculations, notably those of Peterman *et al.*, based on the model proposed by Switendick. Band-structure effects are discussed in detail. Emission from the shallow $3p$, $4p$, and $5p$ core levels are revealed through high-photon-energy spectra. Additional features arising from plasmon losses and Auger emission are shown to be important. For LuH_2 , the $4f$ photoionization cross section is determined, and the probability of bulk-plasmon excitations is shown normalized to the $4f$ cross section.

INTRODUCTION

In this paper we present the results of our photoelectron spectroscopy studies of ScH_x , YH_x , and LuH_x . This study is a continuation of our examination of the electronic states of metal-hydrogen systems.

In two recent papers we discussed studies of the electronic structure of transition- and lanthanide-metal dihydrides as revealed by optical spectroscopy and self-consistent energy-band calculations.^{1,2} In those papers, henceforth termed I (experimental) and II (theoretical), we demonstrated that the often-cited anionic and protonic models failed to describe the electronic structure of the group III dihydrides (or any di or higher-hydride) and that these complex alloys must be examined within the context of one-electron band theory.

In I the interband optical features of ScH_x , YH_x , and LuH_x were studied as a function of composition x , where $x = \text{H}/\text{M}$ ratio, and photon energy $h\nu$ for $0.2 \leq h\nu \leq 5$ eV, using reflectance and thermorelectance techniques.^{1,3} Those results showed the dominance of Drude absorption for $h \approx 1.5$ eV and the importance of interband absorption at higher photon energies.

In II the band model for dihydrides was refined, compared to earlier calculations, by examining the effects of self-consistency and exchange. Those self-consistent bands were compared to the experimental results, and generally

good agreement between theory and experiment was found. [The interband transition features were predicted by theory at somewhat higher energy than observed, but this discrepancy has been reduced in subsequent calculations,⁴ which placed a muffin-tin sphere at the octahedral site (see companion paper to this work).]

The x -dependent experimental absorption features were also discussed in I and II. It was shown that the observed optical structures for low- x dihydrides could be explained in terms of calculations based on the fluorite crystal structure with hydrogen only at tetrahedral sites. The higher- x results ($x \rightarrow 2$) could be understood only by assuming hydrogen occupancy of some octahedral sites before all available tetrahedral sites were filled. Subsequent calculations^{5,6} considered the influence of octahedral occupancy on the band structure. Switendick⁵ considered Y_4H_9 with all tetrahedral sites and one-fourth of the octahedral sites filled, while Peterman *et al.*^{4,6} calculated the electronic energy bands of cubic YH_3 . Both calculations predicted modifications to the fluorite band structure and provided insight into the origin of the observed x -dependent optical structures. Both revealed bands near E_F which were distorted or split by changes accompanying octahedral occupancy. The Y_4H_9 calculation⁵ also offered a plausible explanation for the apparent absence of octahedral protons in ScH_2 but their presence in YH_2 , the difference being related to the position of the antibonding Γ'_2 state relative to E_F and the

second band along Γ - Δ - X . The energy position of Γ'_2 reflects the lattice constant and the consequent H - H spatial separation. These calculations and our experimental studies then demonstrated the propensity of dihydrides with large lattice constants to accept octahedral hydrogen for $x \rightarrow 2$ (Γ'_2 below E_F) while those with smaller lattices such as ScH_2 reject octahedral hydrogen (Γ'_2 above E_F) and do not favor the higher hydride formation. (The reader is referred to I and II for more lengthy discussions of these points.)

In the low-energy optical studies, we probed the bands within a few eV of E_F with conventional laboratory light sources. In order to study the deeper lying bands and continue our quantitative comparison between experiment and the predictions of the one-electron band model, we have pursued extensive photoelectron spectroscopy (PES) studies of these dihydrides, exploiting the tunable, wide-range continuum character of synchrotron radiation. In this paper our emphasis is on the deeper lying bands, since they have until now been largely uncharacterized. Our discussion of the d -band feature near E_F as observed through PES will emphasize the complementary character of PES and optical studies. Throughout our discussion, we will refer to the deeper bands as the "bonding bands," even though not all states in those bands are bonding in character. For example, Γ'_2 is antibonding. A more apt term might then be "covalent," and the distinction should be kept in mind.⁵

In an earlier paper⁷ we discussed the results of our PES studies of ThH_2 and Th_4H_{15} . Those results clearly demonstrated that the bonding bands extend below the d -bands and give rise to strong density-of-states features between ~ 3 and ~ 9 eV below E_F . These bands have mixed angular momentum character, and the degree of hybridization increases as the hydrogen content increases, as for example in the case of ThH_2 and Th_4H_{15} . The thorium hydride system is, however, very complex as far as a detailed band calculation is concerned because the lattice is tetragonal, relativistic effects are important, and the empty $5f$ bands overlap the $6d$ bands.⁸ The hydrides of the group III metals are a more tractable system in which to quantitatively compare the predictions of band theory with experiment. The group III dihydrides are, moreover, prototypes of the other metal dihydrides such as TiH_2 and are free of the tetragonal distortion found in TiH_x or ZrH_x for $x \rightarrow 2$.

EXPERIMENTAL CONSIDERATIONS

We have exploited the intense, continuously tunable, ultrahigh-vacuum compatible character

of synchrotron radiation to study the dihydrides of Sc, Y, and Lu for $15 \lesssim h\nu \lesssim 200$ eV. The work was performed at the Synchrotron Radiation Center, University of Wisconsin-Madison using radiation from Tantalus, the 240-MeV electron storage ring operated for the National Science Foundation as a national radiation facility. Two different optical systems and beam lines were used; both systems had bakeable ultrahigh-vacuum (UHV) monochromators, separation chambers, and mirror boxes which were compatible with the stringent vacuum required for studies of these dihydrides. With our experimental chamber appended to either beam line, we were routinely able to take data at $8\text{--}12 \times 10^{-11}$ Torr within 24 hours of being up to atmospheric pressure (base pressure of isolated chamber $\lesssim 5 \times 10^{-11}$ Torr). For the measurements reported here, the synchrotron radiation white beam was dispersed with a UHV 1-m horizontal Seya-Namioka monochromator ($h\nu \lesssim 45$ eV) or a 2-m grazing incidence "grasshopper" monochromator ($20 \lesssim h\nu \lesssim 200$ eV with 600 lines/mm grating).

The experimental system used for these measurements has been discussed elsewhere.⁹ The PES chamber has standard ports to which a sputter gun, an electron gun, a leak valve, and cleavage tools can be appended, plus numerous other ports for sample inspection and alignment. The samples themselves were mounted on copper holders, which were loaded onto an extra long linear feedthrough, in such a way that 20 or more samples could be loaded at one time for extended runs. The sample manipulator and the double-pass cylindrical-mirror electron energy analyzer (CMA) were mounted on opposing flanges oriented at 78° to the incoming photon beam. The geometry lends itself ideally to studies of the polarization dependence of photoemission features,⁹ but that capability was not used in the present studies of polycrystalline samples. A channeltron with conventional fast electronics was used for counting. Ramping voltages for the CMA were taken either from a programmed power supply or from a Tektronix 4051 computer. Signal averaging and data manipulations were done with the computer; the computer also provided pulses necessary for stepping the monochromators for constant initial-state energy spectroscopy.

The PES samples were prepared and analyzed in the same manner as those studied earlier in our optical studies.^{1,3} For the PES studies, samples were either prepared in the form of posts or posts were cut from the original large optical samples. As described in I, the starting metal material was high-purity, Ames Laboratory Sc, Y, or Lu metal. The samples were polycrystalline with

relatively large (mm) sized grains.

The samples were fractured *in situ* at $\sim 10^{-11}$ Torr with a tungsten cleaver and stainless-steel anvil. At the instant of fracture, the pressure in the chamber increased momentarily owing to the manipulation and scraping of UHV parts (cleaver, anvil, manipulator bellows, etc.), in some cases to as much as 5×10^{-10} , as read from a digital display ion gauge. Samples cleaved at working pressures in the 10^{-11} range showed no evidence of degradation due to hydrogen loss. The results shown herein are typical spectra obtained from many cleaves and repetitive scans for samples of each dihydride.

Immediately after fracture, the samples were moved from the cleaving position to the mutual focus of the photon beam and the CMA, and data acquisition was started. For quantitative analysis of the partial photoionization cross section, the beam current, slit settings, analyzer pass energies, and monochromator throughput were taken into account.

In a series of unpublished preliminary studies of these dihydrides we found them to have highly reactive surfaces. For example, during feasibility measurements, the growth of contamination peaks could be observed in YH_x within minutes at -2.5 eV in the region between the bonding and metal bands, between -5 and -9 eV with maxima at -5.9 and -7.5 eV, and at -11.5 eV when insufficient differential pumping separated the monochromator (a nonbakeable Seya-Namioka monochromator with base pressure of $\sim 10^{-8}$ Torr) and the sample. Similar features were observed during later measurements when the sample was aged overnight at $\sim 6 \times 10^{-11}$ Torr for 18 hours or ~ 4 Langmuirs of exposure to the residual gas background of the chamber.

RESULTS AND DISCUSSION

Photoelectron spectroscopy is a powerful and versatile technique for studying the electronic energy bands of condensed matter, and there have been many fine review articles written which describe the various techniques and applications of PES.¹⁰ In our discussion here we will show that the techniques can be applied to considerable advantage in studies of the dihydrides and that important insight about the initial-state density of states (DOS) can be gained from straightforward analyses of the energy distributions of photoelectrons ejected from the sample following photon absorption.

In our paper on optical studies of these dihydrides we discussed at length the kind of information that can be derived through optical methods.

We also pointed out that optical studies were relatively insensitive to surface effects (\sim a few monolayers) and that bulk properties dominated, an advantage which we exploited by preparing the optical surfaces *ex situ*. In those studies we examined interband effects involving initial and final states within *d*-derived bands within a few electron volts of E_F . In our present PES studies with synchrotron radiation we can probe the deeper states and excite them into states far above E_F , an advantage we did not have in the optical studies.

Photoelectron and optical spectroscopies provide complementary information about the electronic structure or energy states of a system. In PES studies the surface sensitivity is far greater than in our optical studies, and surface contamination of less than a monolayer can ap-

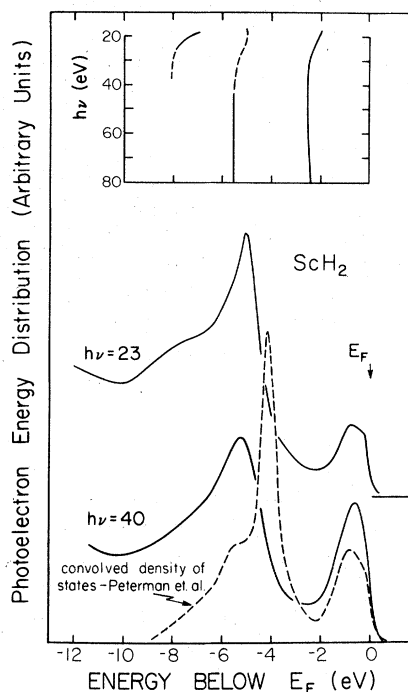


FIG. 1. Photoelectron energy distribution curves (PEDs) for ScH_2 showing the metal-derived band near E_F and the bonding band between ~ 3 and 10 eV below E_F . The upper part of the figure shows the $h\nu$ dependence of the emission features. The loci curves are broken near $h\nu = 30$ eV because of the overlap between Auger emission and direct emission (near the $3p$ core energy). The curve closest to E_F identifies the behavior of the minimum between the metal-derived and bonding bands. The dashed curve gives the convolved density of states for ScH_2 (Ref. 2). The agreement between theory and experiment is improved by better treatment of the potential at the octahedral site as discussed in the text and in the companion paper.

precipitously alter the photoelectron emission spectra. Photoelectrons excited within the uppermost few monolayers, which move to the surface without inelastic collisions, are of primary interest to us here; the scattered or secondary electrons contribute to the background emission.

Select photoelectron energy distributions (PEDs) or energy distribution curves (EDCs) for $\text{ScH}_{1.85}$, $\text{YH}_{1.73}$, and $\text{LuH}_{1.77}$ are shown in Figs. 1–4 for photon energies ranging from 18 to 100 eV. For the sake of presentation and discussion, these spectra have been divided according to the incident photon energy into lower-energy ($h\nu \lesssim 40$ eV) and higher-energy ($h\nu \gtrsim 40$ eV) regimes. In each figure the horizontal energy scale gives the initial-state energy of the photoemitted electron E_i referenced to the Fermi energy E_F . The vertical axis gives the number of electrons of energy E_i for each photon energy $h\nu$, $N(E_i, h\nu)$. N is displayed in arbitrary units, and the spectra are not normalized. Alongside each curve is a label for the photon energy with the monochromator resolution shown for the higher-energy spectra. The electron energy analyzer resolution is ≈ 0.4 eV for the spectra shown. In Figs. 1–3 the emphasis is on the initial states within 12 eV of E_F . The shifting of the maxima or shoulders in the photoelectron energy distributions and the minimum at ~ -2.5 eV are shown at the top of the figures as a function of photon energy to indicate the emission character for photon energies not shown. These loci curves for ScH_2 and YH_2 are dashed in the vicinity of $h\nu = 30$ eV to indicate the uncertainty in the energy identification when Auger emission (involving the np cores and the bonding and conduction bands) overlaps the direct emission features and distorts the spectra. The spectra taken at $h\nu = 40$ eV for ScH_2 and $h\nu = 35$ eV for YH_2 show the Auger emission bands, as shown in Fig. 4. The core levels themselves are shown in Fig. 4 with binding or initial-state energies given relative to E_F . For LuH_2 , the $h\nu$ -dependent photoionization cross section of the $4f$'s is clearly evident from the increasing emission strength of those features with increasing $h\nu$. As shown in Fig. 4, they ultimately dominate the sp - d emission from the sp - d states closer to E_F . The "secondary peak" and emission onset are shown for ScH_2 in Fig. 4 for $h\nu = 40$ eV. These various features will be examined in greater detail throughout the course of the discussion.

Band Structure

The states in the metal-derived or conduction band for dihydrides are relatively insensitive to the hydrogen potential and do not shift significantly

in energy when going from metal to metal hydride.¹¹ Overall d -bandwidth trends for the three isoelectronic dihydrides could then be predicted *a priori* from the d -band behavior of elemental metals; the d bandwidth should increase for the Sc-Y-Lu dihydride sequence. In the optical observations of I interband absorption features involving d -band transitions along Q at E_F were observed to increase in energy from 1.25 to 1.6 to 1.9 eV, and, perhaps more significantly, the W'_2 - W_1 critical-point transitions increased from 2.95 to 3.1 to 3.15 eV for the ScH_2 - YH_2 - LuH_2 sequence. These results directly showed d -band dilation. In the PES results the single conduction-band peak appears at -0.8 eV in ScH_2 , at -1.0 eV in YH_2 , and at -1.1 eV in LuH_2 , and we interpret this feature as being due to emission from the relatively flat band along W - K and nearby regions of k space, as shown in the energy bands of Peterman *et al.* In Fig. 5 we reproduce those YH_2 bands, and we will use them for the present discussions of ScH_2 , YH_2 , and LuH_2 . With that identification of the initial-state energy of the W - K band and the independent optical measure of the W'_2 - W_1 separation we can identify the final-state energy of W_1 as ≈ 2.15 , 2.1, and 2.05 eV above E_F for ScH_2 , YH_2 , and LuH_2 , respectively. These results indicate that the calculated self-consistent bands overestimate the d -band width along Q by ≈ -0.6 eV and at W by ≈ 0.3 – 0.4 eV. Peterman *et al.*^{4,6} have found that, by the inclusion of a muffin-tin sphere at the octahedral site, the d -bands contract, and the agreement with experiment for the Q and W transitions is improved even more. Furthermore, the bonding-band center moves ≈ 0.4 eV away from E_F and closer to the experimental results. Those calculations have been performed only for ScH_2 , and the corrections are not reflected in the bands of YH_2 (Fig. 5).

The densities of states of ScH_2 and YH_2 , as calculated in II and convolved with a Gaussian of full width at half maximum of 0.5 eV, are shown in Figs. 1 and 2 along with the experimental PED's. Because of the relative insensitivity of experimental emission features to $h\nu$, particularly for $h\nu > 40$ eV, a comparison between the PED's and the initial-state DOS's is reasonable. It is important to note, however, that the calculated density of states weights all states equally while the experimental spectra weights different initial states according to their angular momentum character, i.e., their partial photoionization cross section. As can be seen in Figs. 1 and 2, there is good quantitative agreement between the calculated DOS's and the experiment for the metal-derived bands. There is also good semiquantitative agreement for the bonding bands when one compares

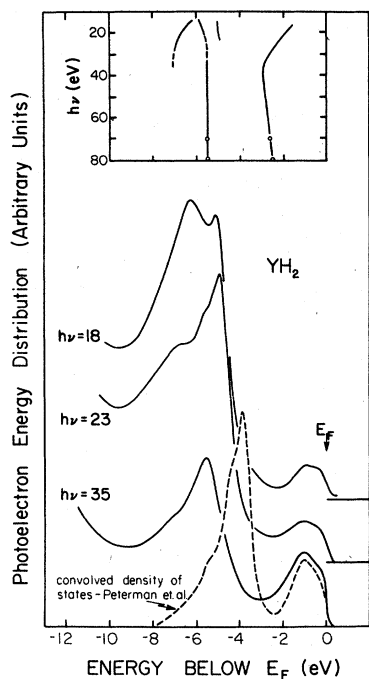


FIG. 2. PEDs for YH_2 . For $h\nu = 23$ eV, three distinct features are visible for YH_2 whereas only two were seen for ScH_2 ; the difference can be related to the dispersion in the bonding bands of the two dihydrides (Figs. 1 and 2 of Ref. 2).

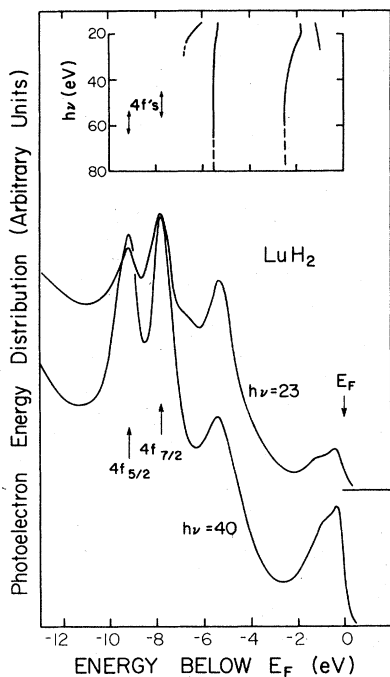


FIG. 3. PEDs for LuH_2 showing the conduction bands near E_F , the bonding bands, and the $4f_{5/2, 7/2}$ features at -7.75 and -9.15 eV.

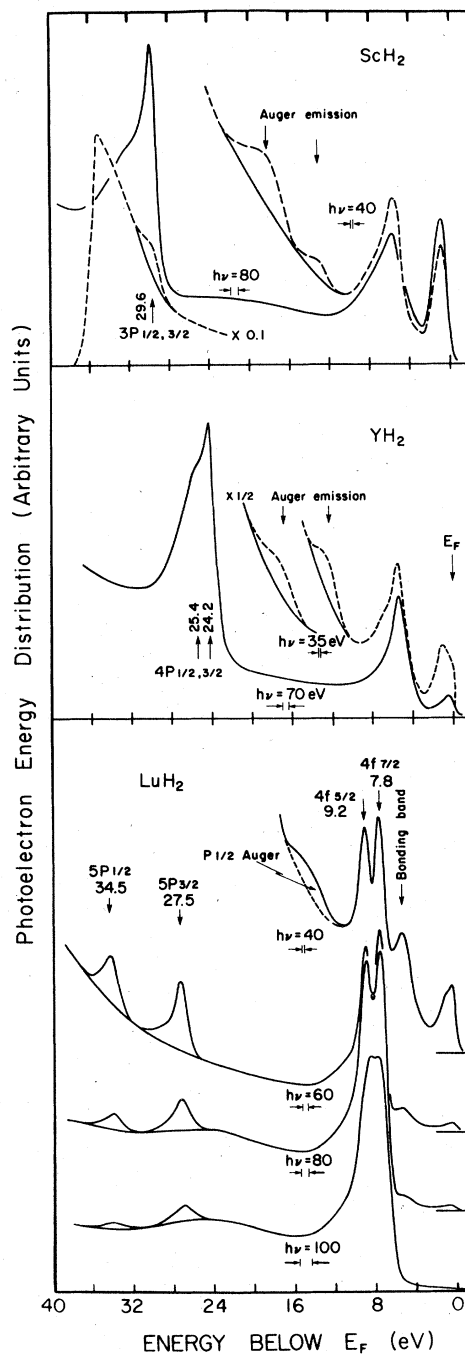


FIG. 4. Higher-photon-energy PEDs for ScH_2 , YH_2 , and LuH_2 showing the conduction and bonding bands and the $3p$, $4p$, $5p$, and $4f$ emission and Auger features, as discussed in the text. The broadening of the core features is attributed to low-energy plasmon losses. In LuH_2 the $4f$ features are shown to be increasingly dominant as $h\nu$ increases above threshold. The broad feature at -24 eV reflects a bulk-plasmon energy loss by the excited $4f$ electron.

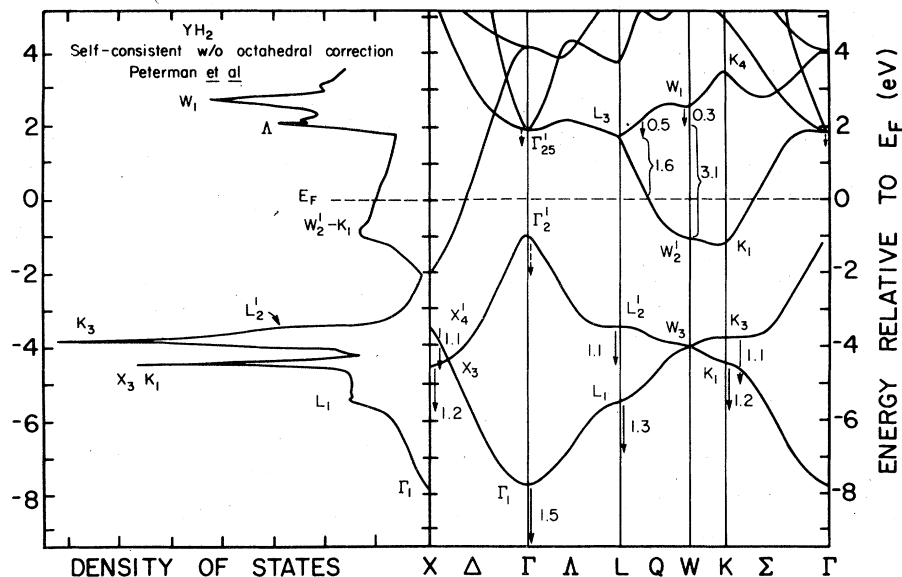


FIG. 5. Self-consistent electronic energy bands and density of states of YH_2 calculated by Peterman *et al.* (Ref. 2) together with initial energies identified through these PES studies and interband separations from the optical studies of Ref. 1. The tip of the arrow indicates the experimental initial state, and its length gives the difference between theory and experiment. As can be seen, the one-electron-band model provides good agreement between theory and experiment. The agreement is improved by the inclusion of a muffin-tin sphere at the octahedral site as discussed by Peterman *et al.* for ScH_2 .

numbers of structures, relative shapes, and general behavior (see, for example, PED's at $h\nu = 23$ eV). Quantitatively, the calculated bonding band center is ≈ 1 eV closer to E_F than observed experimentally, as we will now discuss. Again, this discrepancy is reduced by ≈ 0.4 eV by the inclusion of an octahedral muffin-tin sphere in the band calculation.

The PED's of Figs. 1-3 show the bonding band extending from about -2 eV to about -9 or -10 eV. At low-photon energies the minimum between the bonding and conduction band falls closer to E_F than it does for higher energies. This can best be seen for YH_2 (Fig. 2 loci curve) where the $h\nu$ dependence is greatest; as $h\nu$ is increased from 15 to 37 eV, the minimum shifts from ~ -1.5 to -2.9 eV and then moves slowly back to -2.5 eV for $h\nu \sim 80$ eV. Gradual shifts and changes in dominance of the bonding-band structures themselves can also be seen. Again for YH_2 , the most prominent peak appears at $E_i = -6.3$ eV at $h\nu = 18$ eV, but for higher or lower photon energies, it shifts as shown in the loci curve; as $h\nu$ increases above 35 eV, it gradually vanishes. The peak at $E_i = -5.1$ eV ($h\nu = 18$) shifts toward E_F as $h\nu$ increases, is lost from sight when the strong Auger emission overlaps the bonding band (see, e.g., Fig. 4), and is not observed for higher photon energies. The third bonding-band structure for YH_2 at $E_i = -5.5$ eV is nearly insensitive

to $h\nu$, though at low-photon energy it is masked by the more prominent adjacent structures. At $h\nu = 23$ eV it appears as a shoulder at -5.5 eV, its strength (or visibility) increases as $h\nu$ increases, and above $h\nu = 40$ eV it is the only bonding-band structure observed.

The bonding-band structures of ScH_2 behave analogously to those of YH_2 , as shown in Fig. 1. The lowest YH_2 feature corresponds to the lowest ScH_2 feature, and the other two observed in YH_2 appear unresolved in ScH_2 because the energies of the two initial bands are overlapping. For LuH_2 , there are again two common features with the third unresolved. LuH_2 has two additional structures from the spin-orbit split Lu $4f$'s, which make it impossible to accurately identify the base and the width of the bonding band itself. While the $4f$'s are energetically degenerate with the bonding band, they are highly localized within the atom core, have no appreciable wave-function overlap with the bonding or conduction electrons, and add incoherently to the bonding-band emission. In principle, their contributions could be subtracted, but the errors introduced seem too substantial to justify such a procedure.

The general character of the PED's, their close resemblance to the calculated densities of states, and the relatively slight energy modulation of emission features suggest that we are observing a filtered version of the density of initial states

and that bandlike final states play a relatively minor role at these photon energies. The filters through which the DOS's are seen in experimental photoemission include the $h\nu$ -dependent photoionization process itself, i.e., the variable excitation probability for states of different angular momentum l as a function of photon energy $h\nu$. The calculated DOS has no such "filter" and weights all states equally, as mentioned above. The following few paragraphs reiterate the concepts of cross-section analysis germane to our discussion. We will then use those variations in our interpretation of the experimental structure in terms of the band structure.

Photoionization cross sections have been studied most intently by atomic spectroscopists, and many of the ideas developed by them can be applied with varying degrees of caution to condensed-matter studies.¹² For example, when examining the $h\nu$ dependence of the photoionization cross section $\sigma(h\nu)$ of a localized core state well above threshold where correlation can be neglected, the atomic model is quite reliable. It is also reasonable to use an atomic model when interpreting np - nd or $4d$ - $4f$ photoabsorption in transition metals and lanthanides. However, when considering the cross sections of states in the conduction band especially near threshold, more care is necessary, since those states are not entirely localized and solid-state effects are important. With those cautionary words, we can qualitatively examine the general behavior of emission from the bonding bands of these dihydrides and the cross sections of features within the bands.

The atomic model can be applied most successfully to the highly localized $4f$ states in LuH_2 . As can be seen from Figs. 3 and 4, the $4f$ emission is relatively low at $h\nu \approx 20$ eV (about 10 eV above threshold) but increases steadily and ultimately dominates the other PED features at $h\nu = 100$ eV. The $h\nu$ dependence of the total emission (integrated intensities) of the $4f$ features is shown in Fig. 6. Near threshold $\sigma(4f)$ is small but increases monotonically to a broad maximum ≈ 110 eV above threshold, then decreases.¹² That behavior is consistent with what has been observed for the $4f$'s in Pt and Au.¹³

The delayed maximum in $\sigma(4f)$ shown for LuH_2 in Fig. 4 can be understood by considering the overlap between the localized initial-state wave function and that of the excited continuum g state ϵg ; $4f \rightarrow \epsilon d$ transitions have lower transition probabilities and can be ignored. For low kinetic energies, the ϵg wave function is held out of the region of the $4f$ core by the strong l -dependent centrifugal barrier, the $l(l+1)/r^2$ term in the

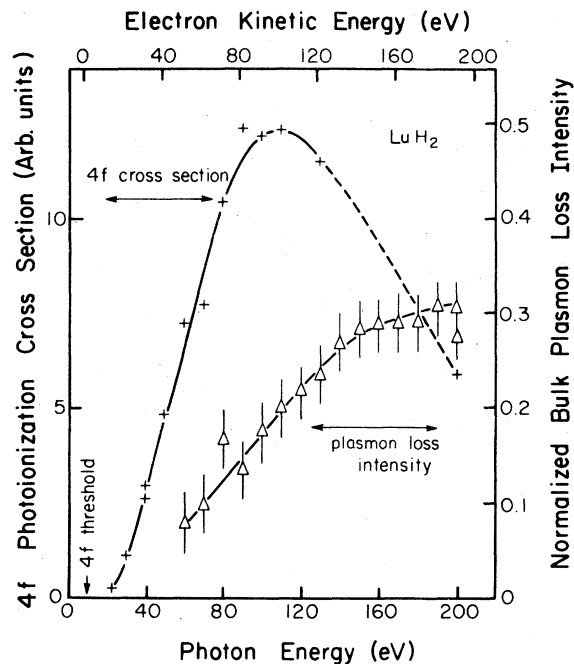


FIG. 6. The partial photoionization cross section for the $4f$ levels in LuH_2 . The $4f$ cross section increased rapidly from threshold ($E_i \approx -8.5$ eV), and the delayed maximum occurs near $h\nu = 85$ eV. As discussed in the text, the excited $4f$ electron can scatter inelastically from a collective resonance or bulk plasmon as it moves through the lattice. The kinetic energy dependence of that loss process (i.e., its intensity normalized by the $4f$ cross section) is shown to increase with kinetic energy and bend over near $E_k = 130$ eV (triangles).

potential. Only as the energy of the ϵg state increases does it overlap appreciably with the $4f$ initial state. The photoionization cross section, which is proportional to $|\langle 4f | r | \epsilon g \rangle|^2$, reflects the overlap and delayed σ maximum. Delayed maxima are also observed for d and p states but are less severely delayed than in f initial states. States of s or p character then can be expected to be most visible in relatively low-photon-energy PED's. As $h\nu$ increases, the cross sections of the higher states increase, those of the lower- l states decrease, and the d or f features dominate. For a more detailed discussion, see Ref. 13 and references therein.

Features in the bonding bands of the dihydrides show $h\nu$ dependences which reflect their initial-state l character, though those states are less atomic than the $4f$'s. Returning to YH_2 and Fig. 2, it can be seen that the deepest and the shallowest bonding-band emission features are most pronounced at low-photon energy but are superseded by the central -5.5 -eV structure for $h\nu \geq 35$ eV. At $h\nu = 35$ eV the deepest feature is still visible as a shoulder at about -7 eV while the shallowest

has vanished. The behavior of the shallowest feature is consistent with s character, and that of the deepest with mixed s - p or s - d character. The central peak can be attributed to largely d -like states. These identifications are supported by the band calculations (next paragraph). It should be noted that if one were to assume that the states in the bonding band were entirely hydrogen-derived with only s character, they would be visible at low-photon energies but would decrease markedly with increasing $h\nu$.

Peterman *et al.*² have calculated the angular momentum character of states at points of high symmetry and along symmetry lines. In Fig. 7 we show their l decomposition of the first two dihydride bands, i.e., the two bands which form the bonding band. From the bands and the experimental results we can make the following identifications:

(i) The states which are responsible for the sharp peak in the calculated density of states of Fig. 5 at $E_i = -3.9$ eV in the calculation are L'_2 , X'_4 , and K_3 and nearby regions of k space. These are nearly degenerate in energy and, as seen in Fig. 7, are largely p -like in the metal sphere and $\approx 100\%$ s -like in the hydrogen sphere; only K_3 has any d character. These bands are responsible for the experimental peak at -4.9 eV ($h\nu = 23$) for YH_2 .

(ii) The shoulder in the calculated DOS arises from the flat portion of the band near L_1 . L_1 is roughly one-third s -like and two-thirds d -like in the metal sphere and s -like in the hydrogen sphere from Fig. 7. Those states near L_1 are the origin of the emission feature observed at about -7 eV. The significant fraction of d character explains why the shoulder is visible at $h\nu \approx 35$ eV.

(iii) The structure at about -4.3 eV in the calculated density of states arises from the bands near W_3 , K_1 , and X_3 . Those states can be compared to the experimental features at -5.5 eV, i.e., with the feature that dominates at high photon energies. Again from Fig. 7, W_3 , K_1 , and X_3 are overwhelmingly d -like, as expected from the PES results.

As can be clearly seen from Fig. 7, there are large portions of the bands *within the bonding band* which have primarily d character in the metal sphere but s character (now shown) in the hydrogen sphere. The experimental results confirm the calculated behavior of these bands: on the formation of a dihydride, metal d states of the appropriate wave-function symmetry are lowered many electron volts and participate in the metal-hydrogen bonding.

The experimental results for ScH_2 and LuH_2 shown in Figs. 1, 3, and 4 can be interpreted analogously to those of YH_2 . The primary dif-

ference observed experimentally is that the bonding band of YH_2 has three features while ScH_2 has only two, and LuH_2 probably has only two. The band structures calculated by Peterman *et al.* show the K_3 , L'_2 , X'_4 states to be nearly degenerate in energy with the bonding-band center (K_1 , W_3 , X_3) for ScH_2 . These are separated by several tenths of an electron volt in YH_2 , as shown in Fig. 5. The energy separation is sufficient in YH_2 to give rise to two experimental PED features, as observed.

The recent, nonrelativistic, non-self-consistent augmented-plane wave (APW) calculations for ErH_2 by Gupta¹⁴ predict that three well-separated DOS features should be observed for ErH_2 at -5.1 , -6 , and -6.7 eV. Except for differences related to the atomiclike $4f$'s, LuH_2 and ErH_2 are nearly identical.¹⁵ We see two features in LuH_2 at -5.5 and about -6.5 eV, which correspond to the calculated structures for ErH_2 at -6 and -6.7 eV. The conduction band is observed to be approximately 2.5 eV wide with a shoulder at -1.1 eV (see Fig. 3) also in good agreement with Gupta's ErH_2 calculations.

Finally, it is interesting to note that the bonding-band energies predicted by the original, non-self-consistent APW calculations of Switendick¹¹ (or Peterman *et al.* and Gupta¹⁴) agree better with experiment than do the bonding-band energies obtained after iterating to self-consistency. The non-self-consistent calculations place the center of the bonding bands within a few tenths of an electron volt of the observed energy of -5.5 eV for YH_2 . When iterated to self-consistency, the calculations shift the bonding bands upward (toward E_F) by ~ 1 eV; see II, Fig. 1 or 2. The inclusion of the muffin-tin sphere at the octahedral site shifts the bonding bands back toward the experimental value and improves the d -band agreement even more, as Peterman and Harmon have shown for ScH_2 in the companion paper.⁴

From the discussion, it should be clear that there is generally very good agreement between the experimentally observed electronic structure of these dihydrides and the results of one-electron first-principles band calculations. That agreement can be seen in Fig. 5 where the self-consistent YH_2 bands are reproduced and indications are made of the modifications that would bring those results into even better agreement with experiment. The octahedral muffin-tin would satisfy the d -band contraction quite well and improve the bonding-band agreement.

Core features, plasmon losses, and Auger emission

As shown with the higher-photon-energy PED's

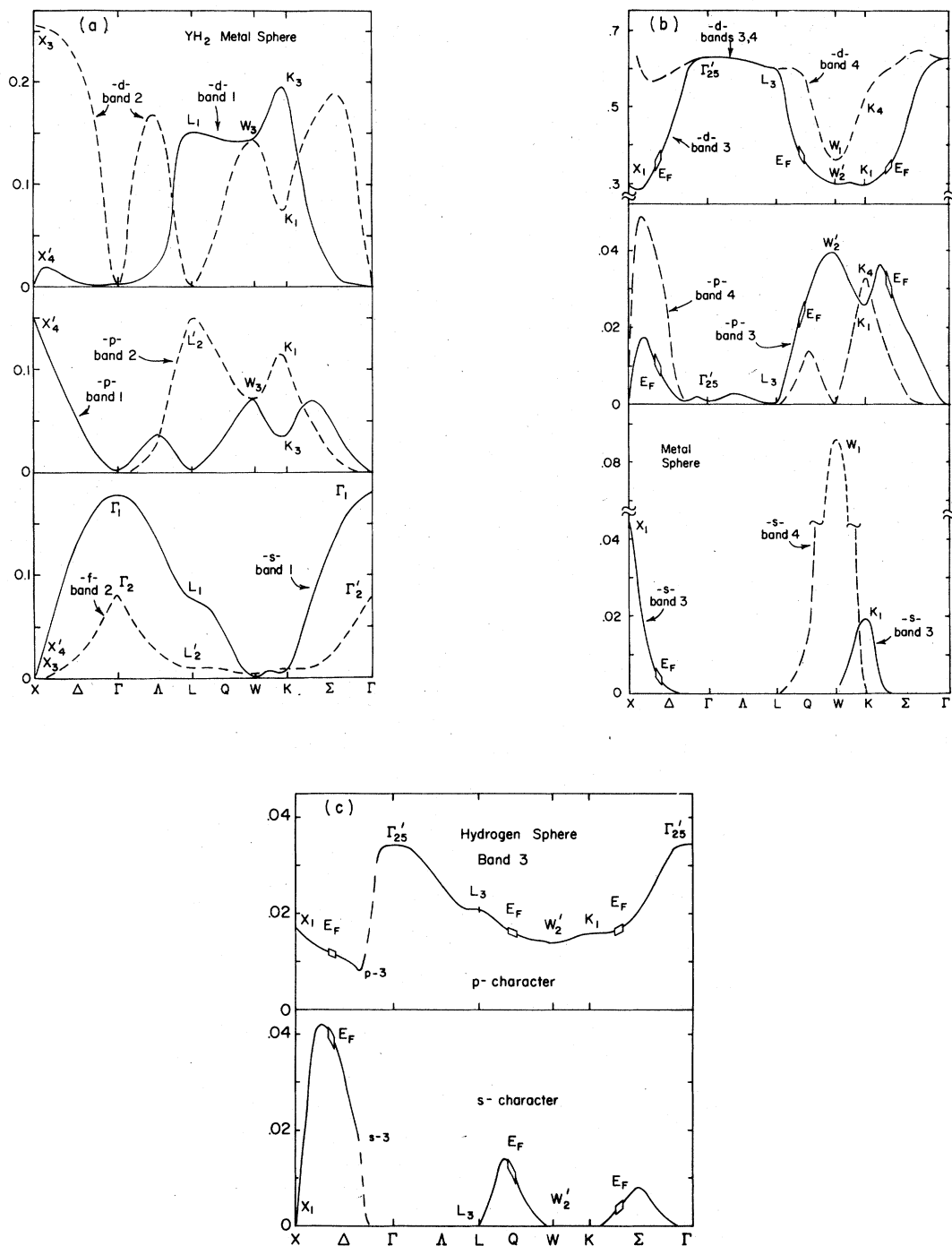


FIG. 7. (a) The angular momentum projection of bands 1 and 2 for YH₂ determined from the results of Peterman *et al.* Bands 1 and 2 constitute the "bonding band." As shown, they have significant amounts of *d* character in the metal sphere; they are *not* purely *s*-like or hydrogen derived but have strong hybridization of hydrogen-*s* and metal-*spd* character. In particular band 1 along L₁-Q-W₃-K₃ is strongly *d*-like, as confirmed by the PES results discussed in the text. (b) The angular momentum projection of bands 3 and 4 in the metal sphere. These bands are overwhelmingly *d*-like. The boxed regions of the curves denote the Fermi-surface crossings, e.g., band 3 along Γ-Δ-X, which is mostly *d*-like at E_F (≈95% *d*-like, 5% *s*- and *p*-like). (c) The *s* and *p* angular momentum projections of band 3 in the hydrogen sphere showing the character of the band at E_F.

of Fig. 4, the $3p$ levels in ScH_2 are 29.6 eV below E_F , the $4p$'s in YH_2 are 24.2 and 25.4 eV below E_F with spin-orbit splitting of 1.25 eV, the $5p$'s in LuH_2 are 27.5 and 34.5 eV below E_F with spin-orbit splitting of 7 eV, and the $4f$'s in LuH_2 are 7.75 and 9.15 eV below E_F with a splitting of 1.4 eV. These energies can be compared to the binding energies for the corresponding pseudocore levels in the metals themselves. Gimzewski *et al.*¹⁶ have reported the $3p$'s of Sc metal to have binding energies of 29.0 ± 0.2 eV. Padallia *et al.*¹⁷ have reported the binding energies of the Lu $5p$'s to be 26.6 and 33.5 eV and the Lu $4f$'s to be 7.6 and 8.9 eV (all energies ± 0.2 eV). There have been no recent studies of the Y $4p$'s. In all cases, if the binding energy of the p core is used as a reference, there is an upward shift of E_F as the metal converts to the hydride by an amount between 0.6 and 1.0 eV. This observation is consistent with what we observed in our studies⁷ of the Th $6p$'s, where we reported that E_F shifted upward by 0.9 eV (measured relative to the $6p_{3/2}$ core) as $\text{ThH}_2 \rightarrow \text{Th}_4\text{H}_{15}$. It is also consistent with the x-ray photoemission spectroscopy (XPS) results of Veal *et al.*,¹⁸ in which they found a chemical shift of ≈ 1 eV toward increasing binding energy for the $4p$'s and ≈ 0.7 eV for the $3d$'s of Zr for $\text{Zr} \rightarrow \text{ZrH}_{1.65}$. They used that observation to argue that there is charge transfer toward the proton site and away from the metal site for ZrH_2 , a conclusion supported by our results and the calculations of II.

Plasmons can be excited either extrinsically by inelastic scattering of an excited electron as it travels to the surface or intrinsically by the potential of a core hole. Identifiable plasmon loss features are observed as companion features to the elastic emission features of the core electrons themselves, separated by $\hbar\omega_p$, the plasmon frequency.

The high-photon-energy spectra for LuH_2 shown in Fig. 4 reveal a broad $h\nu$ -dependent feature centered at $E_i \approx -24$ eV which we interpret as arising from plasmon scattering of the excited $4f$ electrons (centered at -8.5 eV). Empirically, we conclude that the bulk-plasmon energy in LuH_2 is about 15.5 eV. The calculated free-electron plasma frequency for LuH_2 is 14.7 eV.

The bulk-plasmon feature in LuH_2 can be seen most prominently at higher photon energies, as shown in Fig. 4. The $h\nu$ dependence (i.e., kinetic-energy dependence) of the plasmon loss can be quantitatively determined by normalizing the plasmon emission intensity to the $4f$ cross section itself after first subtraction of a background and the $5p_{3/2}$ emission from the PED's. The resulting normalized bulk-plasmon intensity is shown in

Fig. 6 together with the $4f$ photoionization cross section. The energy scale at the top of the figure gives the kinetic energy of the $4f$ electron. As can be seen, even with the relatively large error bars forced by uncertainties in background subtraction, the normalized loss intensity increases steadily for $h\nu \gtrsim 60$ eV and bends over near $h\nu = 140$ eV. This behavior can be compared to the results obtained by Flodstrom *et al.*¹⁹ and Johansson and Lindau²⁰ for Al and Si where a qualitatively similar behavior was observed. That comparison suggests that, by analogy to Si and Al, extrinsic effects are dominant in LuH_2 and more comprehensive studies of loss-related features are in order.

The dihydrides under investigation here exhibit a very strong low-energy bulk plasmon near 1.5–2 eV which has been directly examined through our earlier optical studies. It is the excitation of that low-energy plasmon which we suggest is responsible for the asymmetric broadening of the $4f$ emission feature (see, e.g., Fig. 4, $h\nu = 100$ eV PED). Attempts at determining the photon-energy dependence of that broadening were generally unsuccessful because of the uncertainty in subtracting the background, but those attempts suggest that the normalized intensity is roughly constant over the photon-energy range studied. Finally, the shoulder on the Sc $3p$ structure is probably due to a plasmon loss involving the low-energy plasmon loss in ScH_2 ($\hbar\omega_p = 1.47$ eV); it is not due to spin-orbit splitting of the Sc $3p$ levels, although spin-orbit splitting accounts for the doublet observed for the $4p$'s in YH_2 and the $5p$'s in LuH_2 . Preliminary studies with α ScH_x ($x \lesssim 0.3$), which do not have a low-energy plasmon, do not show the analogous $3p$ core broadening.

The very broad, enhanced emission band centered about -20 eV in ScH_2 can be identified as due to a plasmon loss suffered by the excited d electron; the analogous feature in YH_2 is not visible because of the proximity of the $4p$ core feature. For both ScH_2 and YH_2 , there is a broad structure ~ 13 eV below the np ($n = 3, 4$) emission maximum which can also be related to a plasmon loss. Regrettably, its $h\nu$ dependence could not be observed because the np photoionization cross section drops rapidly and because of the effective upper limit of photon energies available to us with our present 240-MeV storage ring.

The photoexcitation of the shallow p core states makes itself felt in two other ways, which are apparent from the results summarized in Fig. 4. First, two bands of Auger emission are observed which result from the filling of the p core hole by d electrons and the simultaneous ejection of energy-conserving d electrons from the same set

of bands (e.g., $M_{2,3}$, V , V). Since the kinetic energy of the ejected Auger electron reflects only the relative energy positions of the core and the d bands, there is a range of photon energies for which the Auger emission overlaps direct emission from the bonding and conduction bands. This overlap is responsible for the uncertainty in the initial-state energies of the various emission maxima as identified by the loci curves of Figs. 1-3.

Auger decay in these materials is d -band sensitive because of the very strong p - d wavefunction overlap; sp contributions to the Auger current can be ignored. To account for the observed two bands of Auger emission, it is then necessary to postulate two separate bands of d electrons near E_F . (If there were a single band of d states in the conduction band, there would be a single Auger feature with a width given by twice the width of the d band.) Indeed, as we have argued earlier both from the PES direct emission features and from the band-structure calculations themselves, this is what is found in the bonding and conduction bands of the dihydrides. The energy bands within ~ 2 eV of E_F are d derived and the character of those states near the center of the bonding band is strongly d -like. The Auger emission feature close to E_F arises from the two-electron process where both electrons are within the conduction bands (bandwidth ~ 2 eV, Auger emission width ~ 4 eV). The second feature is broader than the first and involves (1) Auger pairs within the d portion of the bonding band and (2) the ejection of one electron from the conduction band when a second electron from the bonding band drops into the p hole. These latter two contributions overlap and result in the relatively wide (~ 7 eV) Auger feature.

The second indirect means by which the p core makes itself felt is a more atomiclike process and will be discussed in more detail elsewhere.²¹ It results from an interference between two paths leading from the initial state of configuration $p^6(ds)^3$ to the final state $p^6(ds)^2 + \epsilon f$, where ϵf denotes an f state in the continuum of energies ϵ . Path one is the direct photoexcitation from a d -band state to the continuum. Path two involves

the creation of the core hole, the strong p hole d -electron overlap and splitting of the intermediate multiplet of states $p^5(ds)^4$, and the decay of the Auger hole with simultaneous ejection of an energetic d state into the continuum. The interference gives rise to a resonance or enhancement of the d -band emission, and the emission of the d band increases between twofold ($6p$ - $6d$ resonance in ThH_2) and 11-fold ($3p$ - $3d$ resonance in ScH_2). As we will show elsewhere, the cross-section resonance can be described by a Fano-type line shape.

SUMMARY

We have shown in this paper that there is generally excellent agreement between the results of a one-electron band calculation for the transition-metal dihydrides with the fluorite structure and experimental PES results. That conclusion endorses the findings of our earlier optical studies of these hydrides and establishes a solid foundation for future studies of the electronic structure of metal-hydrogen systems.

ACKNOWLEDGMENTS

The authors are greatly indebted to the fine support of the Ames Laboratory, USDOE, and the Synchrotron Radiation Center, University of Wisconsin-Madison with special thanks to E. M. Rowe, the director of the SRC, and to H. Baker, A. D. Johnson, R. Otte, D. Klimke, and R. Fasking. The UHV experimental chamber was superbly fabricated by T. Cavallo with expert design support from D. Smithback. The generous loans of equipment by D. E. Eastman, J. E. Rowe, and Z. Hurych enhanced our experimental capabilities immeasurably, particularly during the early phases of this study. We are grateful to G. Margaritondo, N. G. Stoffel, D. J. Peterman, B. N. Harmon, A. C. Switendick, S. H. Liu, R. G. Barnes, and D. Torgeson for numerous discussions and timely assistance. The work was supported in part by the United States Department of Energy, Division of Basic Energy Sciences, and the National Science Foundation (NSF Grant Nos. DMR 77-21888 and DMR 77-07728).

¹J. H. Weaver, R. Rosei, and D. T. Peterson, Phys. Rev. B **19**, 4855 (1979); termed I herein.

²D. J. Peterman, B. N. Harmon, J. Marchiando, and J. H. Weaver, Phys. Rev. B **19**, 4867 (1979), termed II herein.

³J. H. Weaver, R. Rosei, and D. T. Peterson, Solid State Comm. **25**, 201 (1978), a preliminary report of

Ref. 1.

⁴D. J. Peterman and B. N. Harmon, Phys. Rev. B **20**, 5313 (1979); companion paper to this paper.

⁵A. C. Switendick (private communication).

⁶D. J. Peterman, B. N. Harmon, J. Marchiando, and D. Johnson, in Proceedings of the International Conference of Hydrogen in Metals, Münster, 1979 (un-

- published), p. 401; and (unpublished).
- ⁷J. H. Weaver, J. A. Knapp, D. E. Eastman, D. T. Peterson, and C. B. Satterthwaite, *Phys. Rev. Lett.* **39**, 639 (1977).
- ⁸D. D. Koelling and A. J. Freeman, *Phys. Rev. B* **12**, 5622 (1975); E. A. Kmetko and H. H. Hill, *Nucl. Met.* **17**, 233 (1970); J. F. Herbst, R. E. Watson, and I. Lindgren, *Phys. Rev. B* **14**, 3265 (1976).
- ⁹G. Margaritondo, J. H. Weaver, and N. G. Stoffel, *J. Phys. E* **12**, 662 (1979).
- ¹⁰See, for example, the following and references therein: *Photoemission and the Electronic Properties of Surfaces*, edited by B. Feuerbacher, B. Fitton, and R. F. Willis (Wiley, New York, 1978); *Topics in Applied Physics Photoemission in Solids I (II)*, edited by M. Cardona and L. Ley (Springer-Verlag, 1978 (1979), Vol. 26(27); *Electron Spectroscopy, Theory, Techniques, and Applications*, edited by C. R. Brundle and A. D. Baker (Academic, New York, 1977).
- ¹¹See the qualitative bands for fcc Y metal, YH_1 and YH_2 calculated by A. C. Switendick, *Solid State Comm.* **8**, 1463 (1970). See also A. C. Switendick, *Intl. J. Quantum Chem.* **5**, 459 (1971); *Topics in Applied Physics Vol. 28, Hydrogen in Metals: I: Basic Properties*, edited by G. Alefeld and J. Volkl (Springer, Berlin, 1978), p. 101.
- ¹²See, for example, the following and references therein: S. T. Manson, in *Topics in Applied Physics Vol. 26, Photoemission in Solids I; Basic Principles*, edited by M. Cardona and L. Ley (Springer, Berlin, 1978).
- ¹³M. Iwan, W. Eberhard, G. Kalkoffen, E. E. Koch, and C. Kunz [*Chem. Phys. Lett.* (in press)] have recently reported the Pt 4*f* cross section observed through their studies of platinum phtalocyanine. L. I. Johansson, I. Lindau, M. Hecht, S.M. Goldberg, and C. S. Fadley have also reported cross sections for the Au 4*f* [*Phys. Rev. B* **19**, 4126 (1979)]. Note that in the analyses that led to $\sigma(4f)$ of Fig. 6, we have not made a correction for the analyzer efficiency. We feel that the small size of the illuminated sample ($\sim 1 \times 2 \text{ mm}^2$), and the large effective collection area of the analyzer in the XPS mode satisfies the point-source criterion rather than the flooded-source criterion. The correction factor of E_k/E_p for the flooded source would shift the 4*f* maximum toward higher kinetic energy, namely $E_k \approx 80 \text{ eV}$ for the point source.
- ¹⁴M. Gupta, *Solid State Comm.* **27**, 1355 (1978).
- ¹⁵J. H. Weaver and D. T. Peterson (unpublished), PES results for ErH_2 .
- ¹⁶J. K. Gimzewski, D. J. Fabian, L. M. Watson, and S. Affrossman, *J. Phys. F* **7**, L305 (1977).
- ¹⁷B. D. Padalia, W. C. Lang, P. R. Norris, L. M. Watson, and D. J. Fabian, *Proc. R. Soc. London A354*, 269 (1977).
- ¹⁸B. W. Veal, D. J. Lam, and D. G. Westlake, *Phys. Rev. B* **19**, 2856 (1979).
- ¹⁹S. A. Flodstrom, R. Z. Bachrach, R. S. Bauer, J. C. McMenamin, and S. B. M. Hagstrom, *J. Vac. Sci. Technol.* **14**, 303 (1977).
- ²⁰L. I. Johansson and I. Lindau, *Solid State Comm.* **29**, 379 (1979).
- ²¹J. H. Weaver and D. T. Peterson (unpublished). See, for example, the discussions of 4*d*-4*f* resonant photoemission in W. Lenth, F. Lutz, J. Barth, G. Kalkoffen, and C. Kunz, *Phys. Rev. Lett.* **41**, 1185 (1978); L. I. Johansson, J. W. Allen, T. Gustafsson, I. Lindau, and S. B. M. Hagstrom, *Solid State Comm.* **78**, 53 (1978); W. Gudat, S. F. Alvarado, and M. Campagna, *ibid.* **28**, 943 (1978).